Chapter 5
Dielectric Detection Using Biochemical Assays

Yang-Kyu Choi, Chang-Hoon Kim, Jae-Hyuk Ahn, Jee-Yeon Kim, and Sungho Kim

Abstract Point-of-care (POC) diagnostics typically make use of labeling techniques that employ fluorescent, chemiluminescent, redox, or radioactive probes. Although such methods provide high sensitivity, they are complicated because their labeling steps require a significant amount of time and labor in their execution and in the analysis of their results. Thus, the portability, which is meant to be the primary advantage of POC systems, is sacrificed. The use of electronic devices for POC systems circumvents this problem, enabling label-free detection, miniaturization, and low costs. Label-free detection is made possible by direct electrical measurement of the sample molecules, which works by monitoring changes in their intrinsic electrical properties. Miniaturization and the integration of sensors and readout circuitry have been enabled by industrialized microfabrication technology. By integrating the sensors and circuitry onto a monolithic substrate, the fabrication cost can be remarkably reduced.

5.1 Introduction

Point-of-care test (POCT) systems have shown great promise as diagnostic techniques that provide fast, convenient results at or near the site of patient care [1]. These methods, which are widely used, often involve labeling techniques that employ fluorescent, chemiluminescent, redox, or radioactive probes [2]. Although such methods provide high sensitivity, they are complicated because their labeling steps require a significant amount of time and labor in their execution and in the analysis of their results. A transducer that converts a molecular signal to an electrical signal is an indispensible part of the aforementioned approaches, but

Y.-K. Choi (✉) · C.-H. Kim · J.-H. Ahn · J.-Y. Kim · S. Kim
Department of Electrical Engineering, Korea Advanced Institute of Science and Technology, Daejeon, Republic of Korea
e-mail: ykchoi@ee.kaist.ac.kr

D. Issadore and R.M. Westervelt (eds.), *Point-of-Care Diagnostics on a Chip*, Biological and Medical Physics, Biomedical Engineering,
DOI 10.1007/978-3-642-29268-2_5, © Springer-Verlag Berlin Heidelberg 2013

transducers are typically not well miniaturized. Thus, the portability, which is meant to be the primary advantage of POCT systems, is sacrificed. The use of electronic devices for POCT systems circumvents this problem, enabling label-free detection, miniaturization, and low costs [3]. Label-free detection is made possible by direct electrical measurement of the sample molecules, which works by monitoring changes in their intrinsic electrical properties. Miniaturization and the integration of sensors and readout circuitry have been enabled by industrialized microfabrication technology. If the sensors and circuitry are monolithically integrated on the same substrate, then the fabrication cost can be remarkably reduced.

Label-free electrical detection is usually based on the electrical properties of biomolecules. The binding of charged molecules leads to changes in the surface potential, which can be measured by changes in conductivity or capacitance. Although this type of charge-based detection achieves high sensitivity, the sensor signal can be adversely affected by environmental conditions such as pH and ionic strength. Moreover, weakly charged or neutral biomolecules can be difficult to detect with charge-based methods. However, dielectric detection, which is a type of detection based on the dielectric properties of biomolecules, is less sensitive to environmental variations, which allows it to be used to detect weakly charged or neutral biomolecules.

The aim of this chapter is to describe recent advances in the dielectric detection of biomolecules for POCT systems. Several electrical detection techniques will be reviewed. A nanogap-embedded device that is well suited to detecting dielectric changes will be described, and experimental results obtained with this device will be discussed. The discussions will also address the structural modifications of dielectric sensors, different options for sensing metrics, and the effects of environmental conditions on this technology.

5.2 Electrical Detection Based on Dielectric and Charge Properties

5.2.1 Electrochemical Impedance Spectroscopy

Electrochemical impedance spectroscopy (EIS) is suitable for the electrical detection of biomolecular interactions on the transducer surface [4, 5]. In EIS, a voltage perturbation with a small amplitude applied to an electrochemical cell generates a current response. The current response depends on the impedance of biomolecules, which is related to the resistive and capacitive properties of the biomolecules. The impedance is defined as the ratio of the applied voltage and the current response. The impedance between the electrode and the electrolyte solution can be simply modeled using the Randles equivalent circuit, as shown in Fig. 5.1a [4], where R_s denotes the resistance of the electrolyte solution. The charge can be stored in the electrical double layer at the interface, resulting in the double layer capacitance C_{dl}.

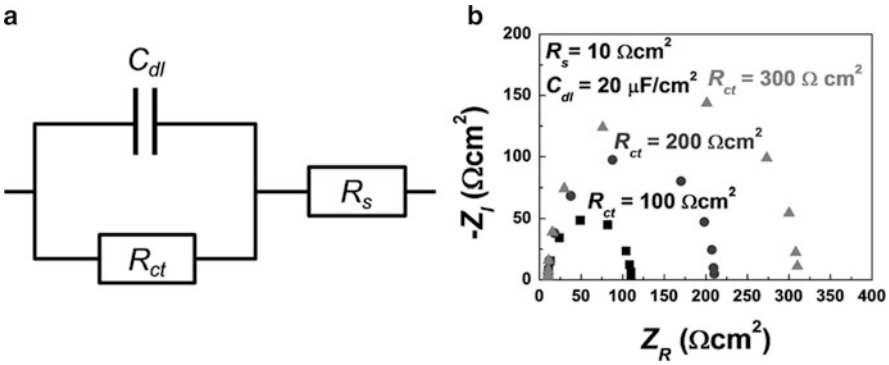

Fig. 5.1 (**a**) The Randles circuit. R_s, C_{dl}, and R_{ct} denote the resistance of the electrolyte solution, the double layer capacitance, and the charge transfer resistance, respectively. (**b**) Nyquist representation of impedance data calculated from the Randles circuit

The charge transfer resistance R_{ct} is related to the current flow caused by the redox reaction at the interface.

Using the resistance R_s in series with the parallel combination of the resistance R_{ct} and the capacitance C_{dl}, as shown in Fig. 5.1a, the total impedance can be given by

$$Z = R_s + \left(\frac{1}{R_{ct}} + j\omega C_{dl}\right)^{-1} = R_s + \frac{R_{ct}}{1 + (\omega R_{ct} C_{dl})^2} - j\frac{\omega R_{ct}\, C_{dl}}{1 + (\omega R_{ct}\, C_{dl})^2}. \quad (5.1)$$

The real part and the imaginary part of the impedance are expressed as

$$Z_{Re} = R_s + \frac{R_{ct}}{1 + (\omega R_{ct}\, C_{dl})^2}, Z_{im} = -j\frac{\omega R_{ct} C_{dl}}{1 + (\omega R_{ct} C_{dl})^2}. \quad (5.2)$$

Impedance data can be represented in Nyquist form as shown in Fig. 5.1b [4]. Each data point corresponds to a different frequency value. The impedance is limited to R_s at high frequencies and $R_s + R_{ct}$ at low frequencies. As shown in Fig. 5.1b, the limited impedance at low frequency increases as R_{ct} increases. The maximum of the semicircle or the maximum of $-Z_{Im}$ occurs when the frequency is equal to $(R_{ct} C_{dl})^{-1}$.

As shown in Fig. 5.2a, receptors, recognition elements, are immobilized on the surface of the transducer electrode. When analytes, target biomolecules, bind to the receptors, the charge transfer between the redox mediator and the electrode is interrupted, resulting in an increased value of R_{ct}. Concomitantly, C_{dl} decreases because the biomolecular thickness increases. By monitoring the impedance change, the binding of the analyte to the receptor at the interface of the electrode can be detected. However, in the presence of the insulator at the interface of the electrode or the absence of the redox mediator, no charge transfer occurs due to the blocking

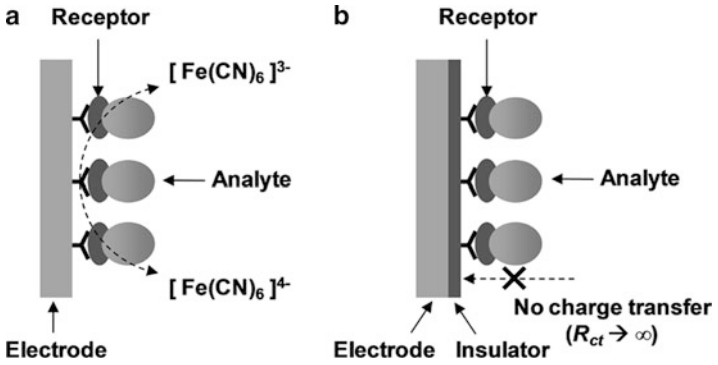

Fig. 5.2 EIS system with (**a**) the redox reaction and (**b**) the blocking of the redox reaction

of the redox reaction, as shown in Fig. 5.2b. In this case, the change in C_{dl} is the only parameter with which to detect analyte binding.

The EIS method has been used for immunoassays [6–8] and nucleic acid detection [8–11]. It is possible to detect target biomolecules with this label-free electrical method, but one of its disadvantages is low sensitivity. Several amplification techniques had been proposed to improve detection sensitivity, including techniques that use enzymes [9, 12], liposomes [13, 14], conducting polymers [15], or nanomaterials [16, 17].

To achieve high sensitivity, a field-effect transistor (FET)-based biosensor has been suggested [18, 19]. Miniaturization and compatibility with complementary metal-oxide semiconductor (CMOS) technology are additional advantages of this type of biosensor. FET-based biosensors are reviewed in the following section.

5.2.2 FET-Based Biosensor

FET-based sensors are attractive because they allow changes in the solution pH or the binding of analytes on the surface to be directly monitored based on changes in the electrical properties of the target molecules.

An ion-sensitive field-effect transistor (ISFET), in which the electrical properties change according to the pH or ionic strength of the solution, was first reported in the 1970s [20]. The structure of an ISFET is shown in Fig. 5.3. An ISFET is essentially a FET in which a gate electrode is replaced by a reference electrode and electrolyte solution. It is noteworthy that the gate dielectric is exposed to the electrolyte solution. The reference electrode supplies a stable potential in the solution and produces a channel under the gate dielectric layer.

The ISFET is not a biosensor but rather a chemical sensor. The gate dielectric of the ISFET, which is a chemically sensitive material, changes the surface potential of the channel depending on the H^+ ion concentration; hence, the source-to-drain

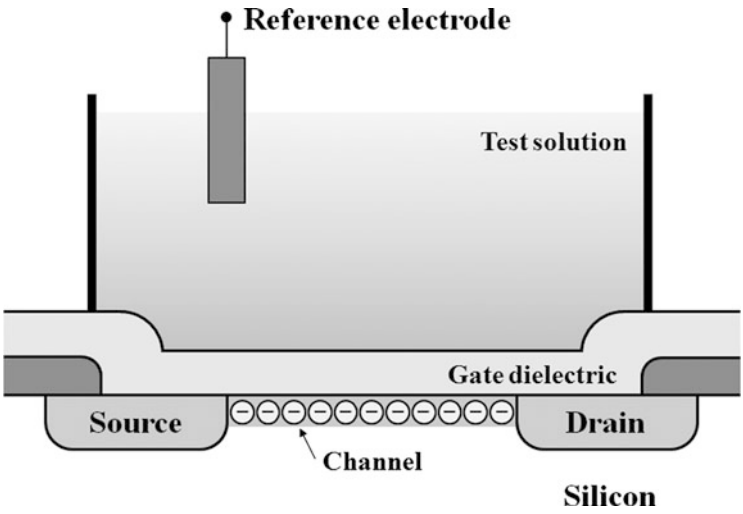

Fig. 5.3 A schematic representation of an ISFET. The reference electrode and electrolyte solution play a role as a gate electrode in an ISFET

current changes [21]. Figure 5.4 shows a typical change in current–voltage characteristics due to the pH changes. Surface hydroxyl groups on the ISFET dielectric layer react with the solution in different ways depending on pH; for a basic solution, this layer shows larger negative charge characteristics compared to an acidic solution. Therefore, the threshold voltage is larger in the case of a higher pH value.

Because the ISFET is very sensitive to any electrical interaction on the surface, it may also be used to detect DNA hybridizations or immunological reactions on the surface. With single-stranded DNAs or antibody/antigen molecules immobilized on the surface, an equivalent threshold voltage change is expected when a specific binding reaction occurs. However, the unreliable operational behaviors of ISFETs have limited their performance as sensors [22]. Unexpected responses such as drift and hysteresis have been observed during sensor operation, resulting in misleading signal changes during measurement. ISFETs are also sensitive to external light and temperature fluctuations [23] as the sensor is made of a semiconductor with a channel area that is exposed to solution. Additionally, the requirement of a reference electrode makes it difficult to build the sensor on a silicon chip using integrated circuit technology.

The limited performance of ISFETs can be overcome by improving the architecture from a planar structure to a nanoscale three-dimensional structure, that is, semiconductor nanowires. Because nanowire has a higher surface-to-volume ratio than a planar device, it displays a higher sensitivity [24]. The molecules bound on the surface affect the channel potential of both devices, but in the case of nanowires, electrical carriers in the bulk of the nanowire are affected as well as in the surface of the nanowire.

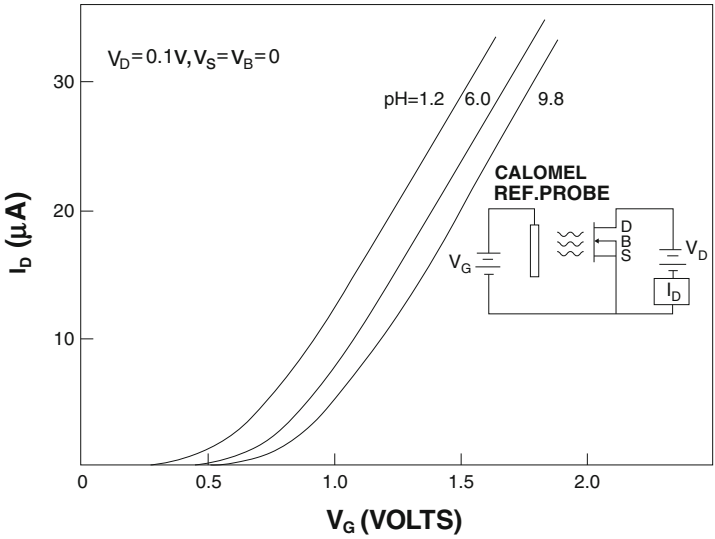

Fig. 5.4 Drain current (I_D) versus gate voltage (V_G) characteristics and their changes with pH. The aqueous solution with the higher pH shows the higher threshold voltage

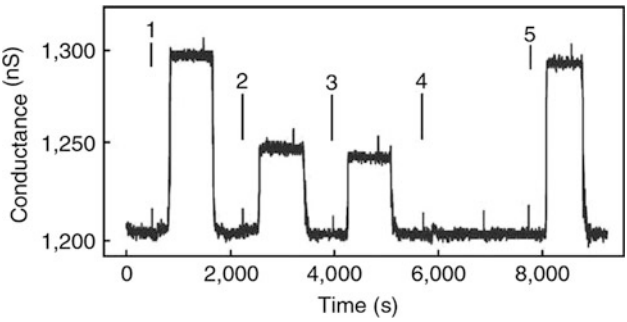

Fig. 5.5 Conductance versus time, recorded for a PSA antibody-modified p-type silicon nanowire for (1) 9 pg/ml PSA, (2) 0.9 pg/ml PSA, (3)0.9 pg/ml PSA and 10 μg/ml bovine serum albumin (BSA), (4) 10 μg/ml BSA, and (5) 9 pg/ml PSA (Copyright 2005 Nature Publishing Group)

Silicon nanowire biosensors have been used to detect ions [24], small molecules [25], proteins [26], DNA [27], and viruses [28] by taking advantage of the changes in surface charge, depending on the binding of target molecules. Surface charges serve as a gate and induce a potential change in the nanowire channel, thus leading to a conductance change in the nanowire. For example, as shown in Fig. 5.5, when prostate specific antigen (PSA), a cancer marker protein, binds to a nanowire coated with the PSA antibody, the conductance is increased because PSA carries a negative charge at pH 7.4.

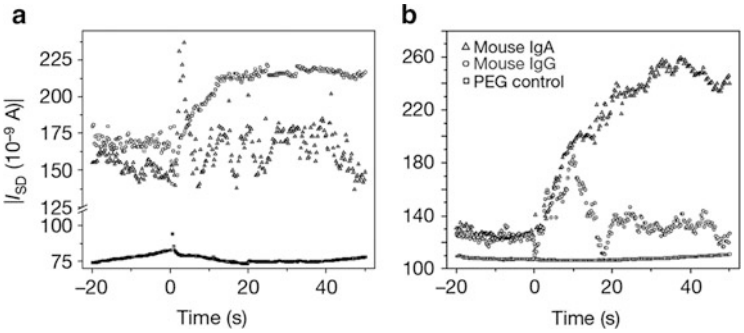

Fig. 5.6 Sensor responses to mouse IgA and mouse IgG for (**a**) goat anti-mouse IgG-functionalized nanowire and (**b**) goat anti-mouse IgA-functionalized nanowire (Copyright 2007 Nature Publishing Group)

In the early days of silicon nanowire biosensor research, "bottom-up" nanowires were widely used. However, in terms of integration, alternative "top-down" fabrication methods are becoming more attractive. The use of "top-down" method has also been demonstrated in a sensor application [29]. The sensor response is shown in Fig. 5.6.

Up to this point, we have summarized electrical detection-based biosensors and dielectric-based biosensors. To utilize both types of sensor technology, a dielectric-modulated field-effect transistor (DMFET) has been suggested. The DMFET has many advantages, such as label-free detection, easy integration of readout systems, compatibility with low-cost CMOS technology, and high applicability for detecting various types of biomolecules, including those that are electrically neutral. The details of DMFET will be explained below.

5.3 Dielectric-Modulated Field-Effect Transistor (DMFET)

5.3.1 Basic Structure and Theory

The DMFET structure can be obtained via the modification of a conventional FET (Fig. 5.7a) [30–32]. The gate is suspended above the gate oxide, and a nanogap is formed by a carving process between the gate and the gate oxide, as shown in Fig. 5.7b. Biomolecules can be introduced and bound within the nanogap using nanofluidics [33]. To create biosensors, a DMFET can be functionalized with receptors (Fig. 5.7c) that capture specific analytes (Fig. 5.7d) in the sample solution. The electrical characteristics of DMFETs are subsequently affected by the properties of the biomolecules introduced into the nanogap; in particular, the charge density and the dielectric constant of the biomolecules alter the electrical properties of the DMFET.

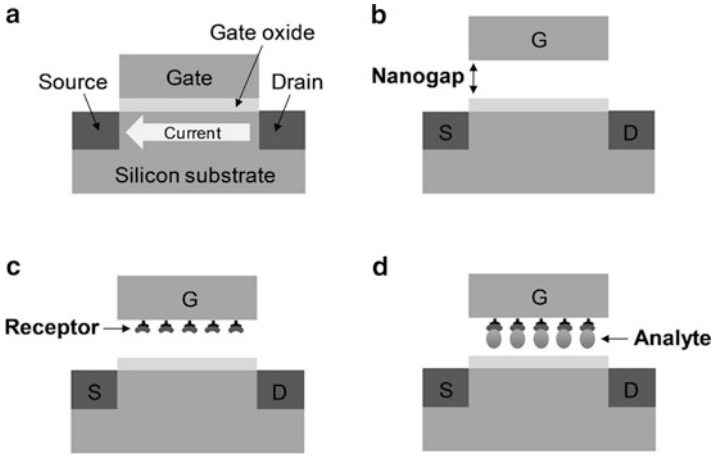

Fig. 5.7 Schematics of (**a**) a conventional FET (**b**) a DMFET with a nanogap between the gate and the gate dielectric (**c**) receptor functionalization in the nanogap, and (**d**) analyte binding on a DMFET

The nanogap is typically fabricated using advanced lithographic techniques such as electron beam lithography and dry etching [34, 35], which make the process expensive and complex. The novelty of the DMFET is its simple nanogap fabrication method, which provides more design flexibility than conventional methods. The nanoscale gap is defined not by lithography but by a thin film deposition and a wet etching process, which are conventional CMOS fabrication methods. The nanogap size corresponds to the deposited thin film, which can be controlled at atomic resolution using an atomic layer deposition (ALD) technique. Thus, the nanogap size is not constrained by a lithographic resolution limit.

When analyzing the effects of biomolecules in DMFETs, an analogy between a conventional FET and the DMFET may be noted. In both cases, the gate voltage (V_G) modulates the drain current, which flows horizontally from the drain (D) to the source (S), as illustrated in Fig. 5.7a. The current starts to flow when the gate voltage exceeds the threshold voltage (V_T). In the operation of conventional FETs, trapped charges in the gate oxide induce a V_T shift. This V_T shift, caused by trapped charges, can be exploited in memory applications [36]. In a similar manner, a V_T shift occurs in DMFETs due to the intrinsic charges of the biomolecules bound in the nanogap. The electrical characteristics of FET are mostly governed by the gate field, which is applied across the gate dielectric. For example, the vertical field from the gate is strengthened as the dielectric constant (k) of the gate dielectric increases. Hence, the drain current can be further increased by the use of a "high-k" gate dielectric material [37]. Similarly, when biomolecules are introduced onto the nanogap of DMFETs, the dielectric constant is increased ($k > 1$) from unity. Thus, it is evident that the dielectric properties of the biomolecules affect the electrical characteristics of DMFETs, especially the threshold voltage and the corresponding drain current.

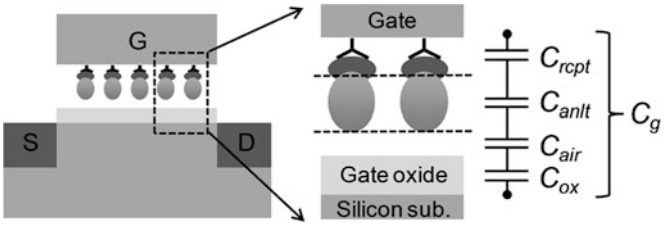

Fig. 5.8 Simplified model of the total gate capacitance (C_g) of a DMFET, corresponding to receptor immobilization and analyte binding. Gate oxide, airgap, analyte, and receptor can be modeled as the capacitances C_{ox}, C_{air}, C_{anlt}, and C_{rcpt}, respectively

To determine the dielectric effect of biomolecules, we initially assume that the analyte is weakly charged or neutral. The V_T value of the DMFET can then be adapted from a modification of the V_T value of a conventional FET and is defined by the following equation:

$$V_T = V_{FB} \pm 2\psi B \pm \frac{Q_{DEP}}{C_g}. \tag{5.3}$$

Here, V_{FB} is the flat band voltage, $2\psi_B$ is the surface potential, C_g is the total gate capacitance, and Q_{dep} is the depletion-layer charge. Equation 5.3 is considered to have a positive sign for n-channel FETs and a negative sign for p-channel FETs. As shown in Fig. 5.8, the gate oxide, airgap, analyte, and receptor can be modeled as the capacitances C_{ox}, C_{air}, C_{anlt}, and C_{rcpt}, respectively. They are connected in series, resulting in the total gate capacitance (C_g) given by the following equation:

$$\frac{1}{C_g} = \frac{1}{C_{rcpt}} + \frac{1}{C_{anlt}} + \frac{1}{C_{air}} + \frac{1}{C_{ox}} = \frac{t_{rcpt}}{k_{rcpt}\varepsilon_0} + \frac{t_{anlt}}{k_{anlt}\varepsilon_0} + \frac{t_{air}}{\varepsilon_0} + \frac{t_{ox}}{k_{ox}\varepsilon_0}. \tag{5.4}$$

In this equation, ε_0 is the permittivity of air, k_{rcpt} is the dielectric constant of the receptors, k_{anlt} is the dielectric constant of the analytes, k_{ox} is the dielectric constant of gate oxide, t_{rcpt} is the thickness of the receptors, t_{anlt} is the thickness of the analyte, t_{air} is the thickness of air, and t_{ox} is the thickness of the gate oxide.

Filling this nanogap ($k = 1$) with analytes ($k_{anlt} > 1$) bound to receptors increases the total gate capacitance and results in a signal change, that is, ΔV_T. According to Eqs. 5.3 and 5.4, ΔV_T can be given as

$$\begin{aligned} \Delta V_T &= V_{T,anlt} - V_{T,anlt} = \pm \left| Q_{dep} \right| \left(\frac{1}{C_{g,anlt}} - \frac{1}{C_{g,anlt}} \right) \\ &= \pm \left| Q_{dep} \right| \left(\frac{t_{anlt}}{k_{anlt}\varepsilon_0} - \frac{t_{anlt}}{\varepsilon_0} \right) = K \left(\frac{1}{k_{anlt}} - 1 \right) \end{aligned} \tag{5.5}$$

where $K = \pm |Q_{dep}| t_{anlt} / \varepsilon_0$ denotes the response coefficient. Again, the equation has a positive sign for n-channel FETs and a negative sign for p-channel FETs.

Table 5.1 The direction of V_T according to the properties of biomolecules and the types of FETs

		n-Channel FETs	p-Channel FETs
Dielectric effect		$\Delta V_T < 0$	$\Delta V_T > 0$
Charge effect	Negative	$\Delta V_T > 0$	
	Positive	$\Delta V_T < 0$	

Thus, it is possible to detect the specific bindings of biomolecules by monitoring ΔV_T. As shown by Eq. 5.5, the amount of signal change increases as the dielectric constant of the analyte (k_{anlt}) increases. Moreover, the signal change can be enhanced via the response coefficient, which is determined by t_{anlt} and Q_{dep} that, in turn, depend on the substrate doping concentration. Although we previously assumed that the analyte is weakly charged or neutral, strong charges exist on some of the most analyzed biomolecules: proteins and nucleic acids. When the analyte is negatively/positively charged, it leads to a positive/negative V_T shift ($\Delta V_T > 0/\Delta V_T < 0$) in both n-channel FETs and p-channel FETs.

It is important to note that the direction of the V_T shift depends on the dielectric and charge effects of the biomolecules, as well as the types of FETs, as shown in Table 5.1. Thus, the properties of the biomolecules and the device type should be considered to maximize the signal change.

It is well known that the charge effect is inversely proportional to the distance from the sensor surface (here, the channel). As the charged analytes move far from the silicon channel, the charge effect tends to be weaker, resulting in a smaller V_T shift. Thus, one should consider a binding site where receptors are immobilized and subsequent analytes are bound. When the binding site is close to the silicon channel, the charge effect is the dominant factor, exceeding the dielectric effect. However, when the binding site is far from the silicon channel, the charge effect is weaker, and the dielectric effect is relatively more influential in the detection of the analytes. Additional details and experimental data are described in the following section.

5.3.2 Proof of Concept and DNA Detection with DMFET

The first result involving a DMFET was reported in 2007 [30]. In that work, researchers concentrated on the proof of concept of a DMFET with weakly charged biomolecules: specifically biotin and a streptavidin biomolecules, which are the most widely used biomolecules in verifications of the operation of a biosensor. The fabricated DMFET had a thick gate oxide (10 nm) and a gold gate with nanogaps at the edges of the gate dielectric, as depicted in Fig. 5.9. The thick gate dielectric reduced the V_T shift caused by trapped charges or intrinsic charges from biomolecules; hence, only a V_T shift due to a change in the dielectric constant was, in fact, observed (Fig. 5.10).

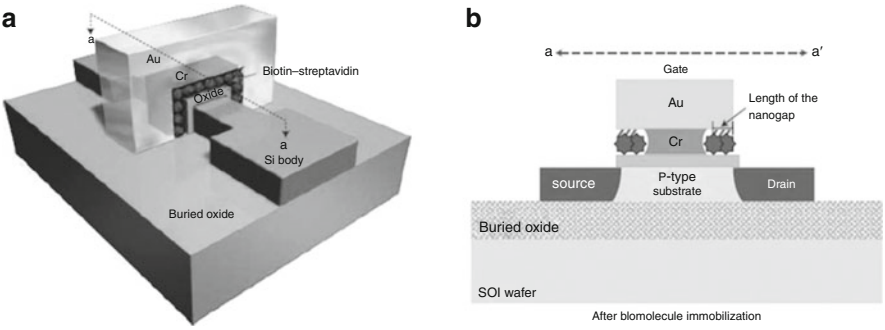

Fig. 5.9 (**a**) 3D schematic and (**b**) cross-sectional structure of a DMFET (Copyright 2007 Nature Publishing Group)

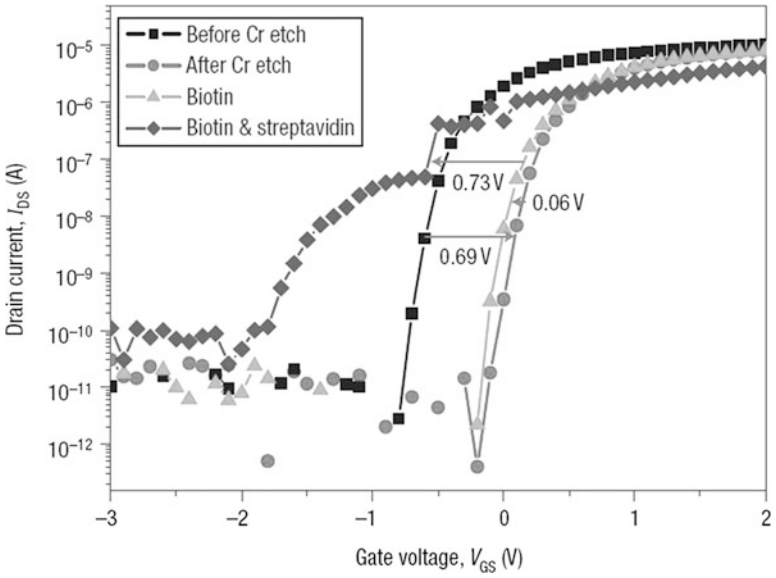

Fig. 5.10 Shows the sequential V_T shift according to the biomolecule binding steps. As mentioned previously, V_T was shifted in the positive direction in an n-channel DMFET after the formation of the nanogap, which occurred because the dielectric constant of the dielectric layer was reduced. However, the positively shifted V_T returned to a negative value because the dielectric constant was increased from 1 to a higher number ($k > 1$ for biomolecules). As shown in Fig. 5.10, the V_T shift after the binding of streptavidin and biotin was 0.73 V (Copyright 2007 Nature Publishing Group)

The subsequent research on DMFETs concentrated on the charge effect related to the V_T shift [38]. To maximize the V_T shift caused by trapped charges or intrinsic charges, a newly designed DMFET with a very thin gate oxide (4 nm) was fabricated. Two types of devices, an n-channel DMFET and a p-channel DMFET, were fabricated at the same time to verify the charge polarity effect according to

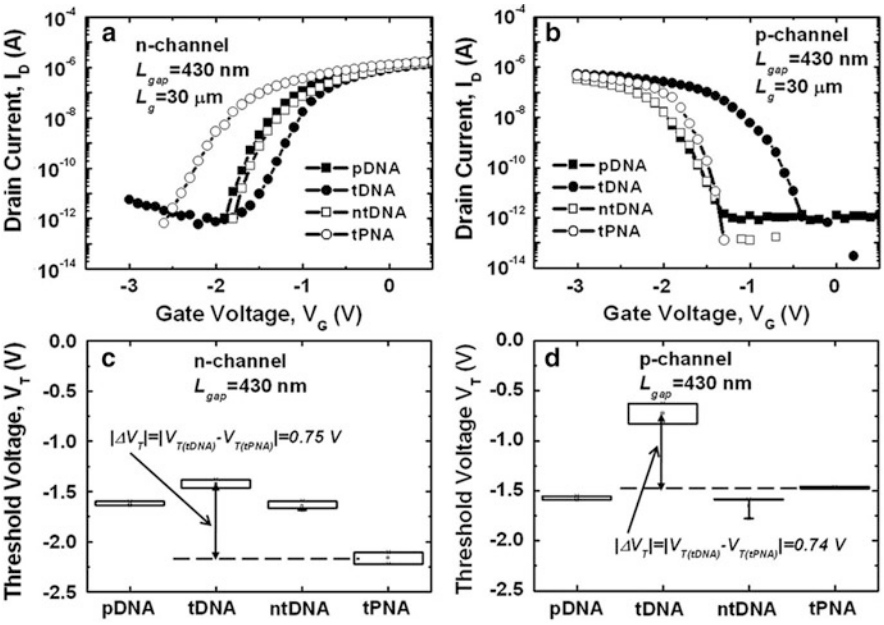

Fig. 5.11 Transfer characteristics (I_D–V_G) of (**a**) an n-channel and (**b**) a p-channel DMFET for a targeted workgroup and various control groups. Statistical variation of V_T shifts for target DNA, noncomplementary target DNA, and target PNA hybridizations in (**c**) an n-channel and (**d**) a p-channel DMFET (Copyright 2011 IOP Publishing Ltd)

the type of FET. The target biomolecules were also replaced with DNA, which is a negatively charged biomolecule. PNA, which has no electrical charge, was used for control experiments to verify the dielectric constant effect.

Figure 5.11 shows the transfer $I_D - V_G$ characteristics and statistical variation of V_T according to the biomolecule binding steps for the n-channel and the p-channel DMFETs. In the graphs, the charge effect and the dielectric constant effect counteract each other in the n-channel DMFET, whereas they are acting in the same direction to shift V_T in the p-channel DMFET. With these data, it was verified that the dielectric constant increment and negative charges in DNA were competing against each other in the n-channel DMFET, as shown in Table 5.1. The V_T value of the p-channel DMFET shifted toward the positive side either after target DNA (analyte) or target PNA (analyte) hybridization, whereas the V_T value of the n-channel DMFET shifted to the positive side only when the target DNA was hybridized. In addition, it shifted to the negative side when the target PNA was hybridized to probe DNA (receptor). A notable result was that the differences in the V_T shift between the PNA hybridization and DNA hybridization to the probe DNA had the same value, indicating that the differences were entirely caused by the negative charges in the DNA. From this result, it was confirmed that an increment in the sensing margin is possible via the proper selection of the FET type, that is, n- or p-channel, according to the charge polarity of the analyte.

5.4 Structural Modification of a DMFET

5.4.1 Underlap FET

The DMFET has the advantages of high compatibility with the conventional CMOS process and adaptability to readout circuits for on-chip integration; however, the bio-reaction probability is lower than that of other biosensors because the sensing part in a DMFET is retracted and covered by the gate material. To overcome this shortcoming while maintaining the advantages of the DMFET, an underlap FET was proposed (Fig. 5.12) [39]. With a novel structure derived from a conventional FET, the underlap FET has all of the merits of the DMFET, as well as additional advantages originating from the underlap structure [39]. The underlap structure shows higher bio-reaction probability and structural stability compared to the carved nanogap architecture due to its opened sensing area. In addition, small changes in the current can be accurately measured because the channel potential in the underlap region is highly sensitive to external charges [39].

Figure 5.12 shows a schematic of the underlap FET in which an offset (underlap region) is introduced between the gate and the drain. The underlap region serves as the sensing area; target molecules on the underlap region will affect the channel potential of the underlap region, which results in a drain current change.

For more details, see Fig. 5.13, which shows an expanded view of an underlap FET to explain its operational principle. After the immobilization of charged biomolecules on the underlap region, the number of inverted electrons in the underlap region is modulated, thus causing a conductance change to occur. As a result, the drain current at a particular gate voltage will change.

The operation of an underlap FET was demonstrated using an avian-influenza (AI) antigen/antibody. As shown in Fig. 5.14, after the binding of the AI antibody (anti-AI), the drain current was significantly decreased. The abrupt drop in drain current was attributed to the negative charges of the anti-AI: negatively charged molecules increase the channel potential, resulting in a decrease in the drain current.

With its simple fabrication process, CMOS process compatibility, and enhanced sensitivity, the underlap FET is a promising candidate for use in chip-based biosensors.

5.4.2 Double-Gate FET

As mentioned previously, there have been two main approaches used in preparing nanowire biosensors: bottom-up and top-down [40]. In the bottom-up process, integration issues and incompatibilities with the conventional CMOS process cannot be avoided, even though the size of the nanowire can be reduced beyond the limit of lithographic resolution. In contrast, the top-down approach is restricted by the lithographic resolution limit, but it enables more precise control of the position

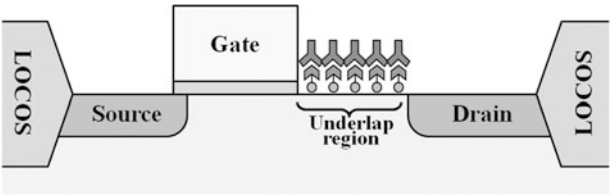

Fig. 5.12 A schematic of an underlap FET. The underlap region is introduced between the gate and the drain; this region serves as a sensing area

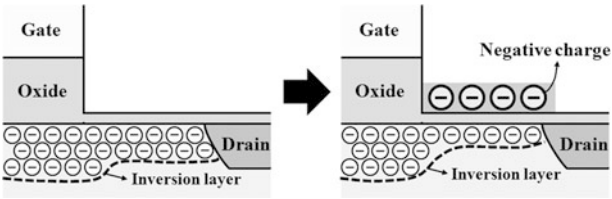

Fig. 5.13 Expanded view of an underlap FET

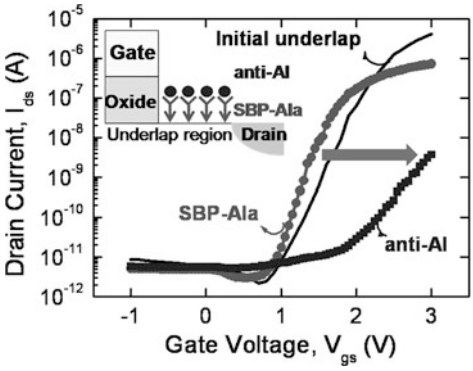

Fig. 5.14 Bio-experimental results obtained using an underlap FET. *Circular dots* indicate the $I - V$ characteristics of SBP-AIa, and *square dots* show the same characteristics for anti-AI (Copyright 2010 American Institute of Physics)

of the nanowire and enables the fabrication of perfectly ordered nanowire arrays [41]. Thus, it is timely to consider the structural and/or operational modifications of nanowire biosensors to overcome the aforementioned challenges while also utilizing the well-established CMOS technology.

A double-gate nanowire biosensor was proposed to avoid the aggressive scaling of silicon nanowires in biosensor applications [42]. Compared to conventional nanowire FET biosensors, which are operated using a single bottom gate, the remarkable difference in the double-gate FET is that independent double gates (G1 and G2) are positioned vertically beside the silicon nanowire and facing each other, as shown in Fig. 5.15.

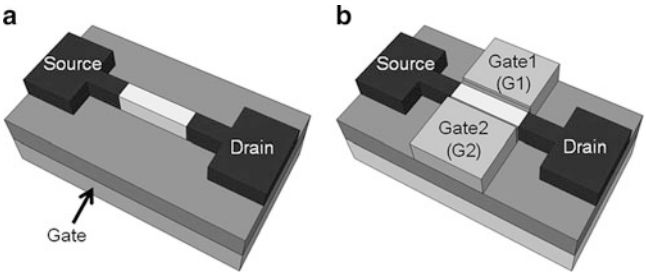

Fig. 5.15 Schematics of (**a**) a conventional nanowire FET and (**b**) a double gate nanowire FET

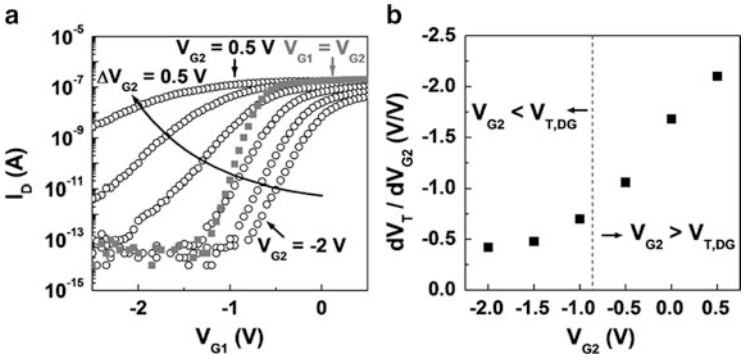

Fig. 5.16 (**a**) $I_D - V_{G1}$ for various V_{G2} conditions and (**b**) impact of the change in V_{G2} on the change in the threshold voltage (Copyright 2010 American Chemical Society)

There are two ways to drive the FET in the double-gate structure: the single-gate (SG) mode and the tied double-gate (DG) mode [43]. In the SG mode, G1 is used as a drive gate, and G2 is used as a supplementary gate to pin the channel potential at a fixed voltage. In contrast, in the DG mode, G1 and G2 are electrically connected, which implies that the same voltage is always applied to G1 and G2; that is, it has a symmetrical bias ($V_{G1} = V_{G2}$).

The data measured in the SG mode (hollow circles) in Fig. 5.16a show that the drain current by G1 can be modulated according to the bias condition of G2. The increment of the G2 voltage (V_{G2}) from a negative to positive value tends to lower the V_T value and degrade the subthreshold slope (SS), which is defined as $d(V_{G1})/d(logI_D)$; that is, it becomes less steep. However, the characteristics of the DG mode (filled squares) show a steeper SS than that of the SG mode due to the greater control over current in the double – gate FET [43].

As shown in Fig. 5.16b, when V_{G2} is larger than $V_{T,DG}$ (V_T in the DG mode), V_T changes significantly in response to small changes in V_{G2}. However, changes in V_T are less sensitive to V_{G2} when V_{G2} is lower than $V_{T,DG}$. Thus, the sensitivity in terms of V_T is less affected by the condition of V_{G2}.

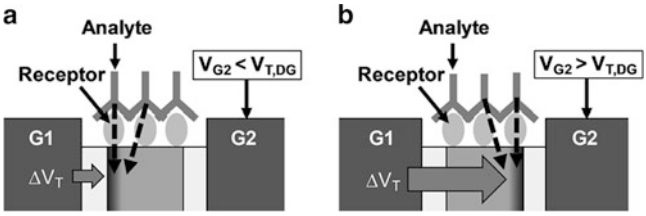

Fig. 5.17 A schematic explaining the effect of different V_{G2} conditions on the V_T shift in biosensing applications. V_T changes occur because the channel is electrostatically affected by the charge of the analyte, which is bound to the receptor. (**a**) $V_{G2} < V_{T,DG}$. Given that the channel is formed close to the G1 side, G1 can easily control the channel, leading to a small V_T shift. (**b**) $V_{G2} > V_{T,DG}$. The channel is induced on the G2 side. The V_T shift increases due to the relatively large distance between G1 and the channel (Copyright 2010 American Chemical Society)

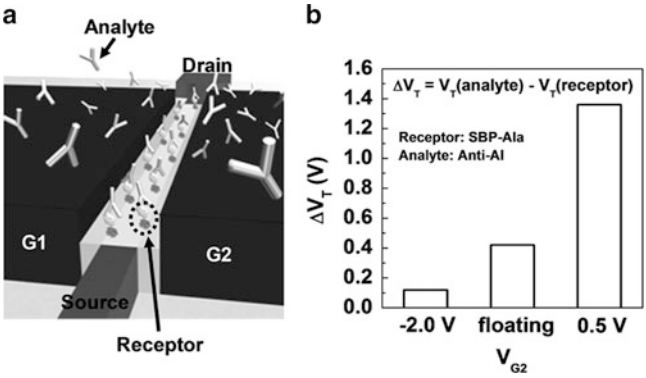

Fig. 5.18 (**a**) A schematic of a double-gate nanowire FET with immobilized biomolecules and (**b**) V_T shift due to target molecule binding versus various V_{G2} conditions (Copyright 2010 American Chemical Society)

As shown in Fig. 5.17, charged analytes (e.g., antibodies) bound to receptors immobilized on the nanowire attract/repel the inversion layer (channel) depending on their charge polarity. In this way, the V_T value is changed. As shown in Fig. 5.17a, because the channel is formed close to the G1 side under the condition of $V_{G2} < V_{T,DG}$, G1 can control the channel efficiently, resulting in a small ΔV_T value. Under the condition of $V_{G2} > V_{T,DG}$ as shown in Fig. 5.17b, however, the channel is relatively far from the G1 side; hence, G1 loses its ability to control the channel conductivity, leading to a large ΔV_T value [44].

To test sensing ability, bio-experiments using a specific analyte-receptor binding system for the detection of the anti-AI were performed, as shown in Fig. 5.18a. An AI antigen (AIa) fused with silica-binding protein (SBP) was immobilized on the surface of the nanowire via the SBP domain which serves as an anchor. The specific binding between SBP-AIa and anti-AI was then accomplished by introducing anti-AI onto an SBP-AIa immobilized device.

The inherent negative charges of anti-AI increase the V_T and lead to a positive V_T shift, as shown in Fig. 5.18b. When a V_{G2} value of -2.0 V ($< V_{T,DG}$) is applied, there is no remarkable change in V_T. In contrast, V_T changes significantly when a V_{G2} value of 0.5 V ($> V_{T,DG}$) is used. It is noteworthy that this bias condition shows enhanced sensitivity compared to the condition of a floating V_{G2}, which is the most similar to a conventional single-gate nanowire FET.

Even for the same nanowire dimensions, the double-gate nanowire FET with a supportive gate (G2) can deliver enhanced sensitivity compared to the single-gate nanowire FET. Thus, the difficulties in scaling down nanowire biosensors can be overcome by implementing a double gate using matured CMOS technology.

5.5 Sensing Metrics in a DMFET

Currently, the detected response from FET-based biosensors, that is, the sensing parameter, is always a V_T shift. However, this restricted sensing scheme leads to several problems: (1) The scope of possible analyses is limited because only the detection of biomolecules themselves is possible. An attempt to calculate the charge-trapping properties of DNA using the V_T shift was made [45]; however, this did not provide any physical or electrical meaning about the DNA regarding the amount of the trapped charge. (2) In addition, as only a small amount of electrostatic force under a low concentration of target molecules participates in the biosensing procedure, the net response is generally less than an order of magnitude; thus, this type of sensing scheme is associated with a low signal-to-noise ratio [46]. To improve the sensitivity relative to noise, the dimensions of the sensor device must be scaled down, which complicates the fabrication of the device [47].

Actually, a FET has many useful and sensitive device parameters aside from V_T. Every device parameter can be utilized as a sensing parameter for detecting biomolecules. In this section, new sensing parameters for use in a DMFET are discussed.

5.5.1 Interface Trap Charge Method

One device parameter that can be utilized as a sensing parameter is the number of interface states at the surface of the channel, or the channel/gate dielectric interface (normally Si/SiO_2), which is also referred to as the interface trap density (D_{it}). The interface trap is a very sensitive parameter that can affect the device characteristics severely. Therefore, many techniques to investigate and extract D_{it} electrically have been developed; among them, charge-pumping [48] and $1/f$ noise measurements [49] have been studied since the 1960s. A recent and related development is the advent of a biosensing technique that detects the interface state modulation resulting from biomolecular interactions.

In this section, two newly developed sensing techniques for FET-based biosensors, charge-pumping [50–53], and $1/f$ noise measurement [54] are discussed. Their advantages and weaknesses, operation principles, and technical issues are also described.

5.5.1.1 Charge-Pumping Technique

The operating principle of the charge-pumping technique is as follows: a DMFET is fabricated in which the gate dielectric is partially etched to form a nanogap, as shown in Fig. 5.19a. Interface traps are located at the interface between the channel and the gate dielectric, and the measured charge-pumping current (I_{CP}) is proportional to the interface trap density [55]. Therefore, because the nanogap exposes the silicon channel to biomolecules directly, additional traps can be provided by biomolecules immobilized inside the nanogap; consequently, variation of the trap density can occur with a measurable quantity (I_{cp}) that is highly sensitivity.

The great advantage of the charge-pumping technique is its sensitivity; when the frequency and the level of the applied pulse were optimized by the prediction from the derived analytical model [52], the micro-sized FET showed high sensitivity that was comparable to a nanowire biosensor without a dimension scaled to the nanoscale. This makes the fabrication of a highly sensitive biosensor at a low cost feasible. Figure 5.20 shows the measured values of I_{cp} as a function of the charge-pumping frequency (f_{cp}). It was verified experimentally that the sensitivity can be improved if a lower pulse frequency is used during the charge-pumping measurement [52]. The sensing margin can be improved if f_{cp} is lowered; consequently, the sensitivity can fall below the picomolar concentration regime without scaling the physical size of the sensor.

Another advantage is that the charge-pumping technique is able to analyze various properties of biomolecules electrically. Hence, not only does it enable the detection of biomolecules, but it also extracts their fundamental electrical properties. For example, the identification of the biomolecular charge polarity was demonstrated using a charge-pumping technique [53]. When negatively or positively charged biomolecules are immobilized in the nanogaps, the V_T of a FET is not uniform along the channel but instead varies locally, as shown in Fig. 5.21a. Accordingly, if the maximum peak level of the pulse (V_h) is increased gradually, a lateral V_T profile can be expected. Consequently, the biomolecular charge polarity can be identified. The experimental results are provided in Fig. 5.21b and c, showing that the biomolecular charge polarity was successfully determined by the shift of the direction of the $dI_{cp}/dV_h - V_h$ curves. Therefore, the charge-pumping technique is useful in that it enables the analysis of various electrical properties of biomolecules and can be utilized as an investigational tool to extract their fundamental properties and their biosensing characteristics.

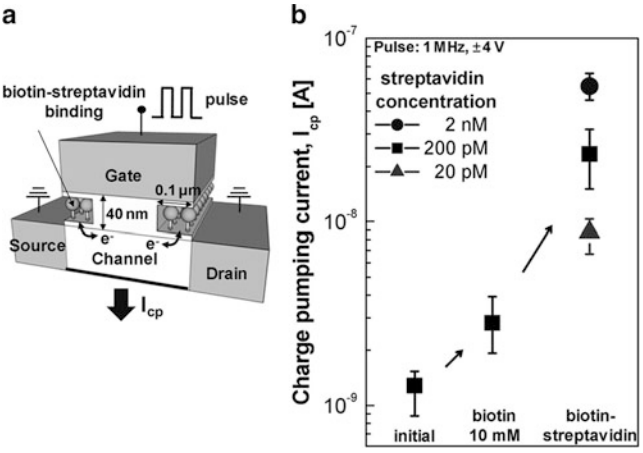

Fig. 5.19 (**a**) A schematic diagram of a DMFET and the experimental setup for the charge-pumping measurements [52]. (**b**) Experimental results comparing the measured I_{cp} values before and after the binding of biotin-streptavidin in the nanogap. When the concentration of a biotin/phosphate-buffered saline (PBS) solution is fixed at 10 mM, the modulation of I_{cp} depends on the streptavidin/PBS solution concentration, which ranged from 20 pM to 2 nM in this case [51] (Copyright 2010 American Institute of Physics)

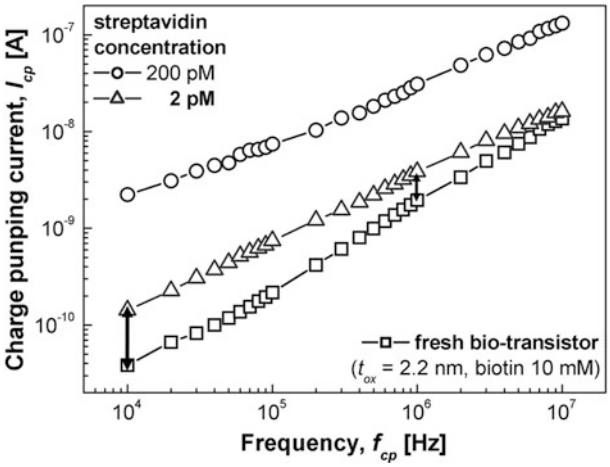

Fig. 5.20 Measured I_{cp} values as a function of the frequency. The sensing margin is increased in the low-frequency range. The sensitivity can fall below the picomolar concentration range [52] (Copyright 2010 American Institute of Physics)

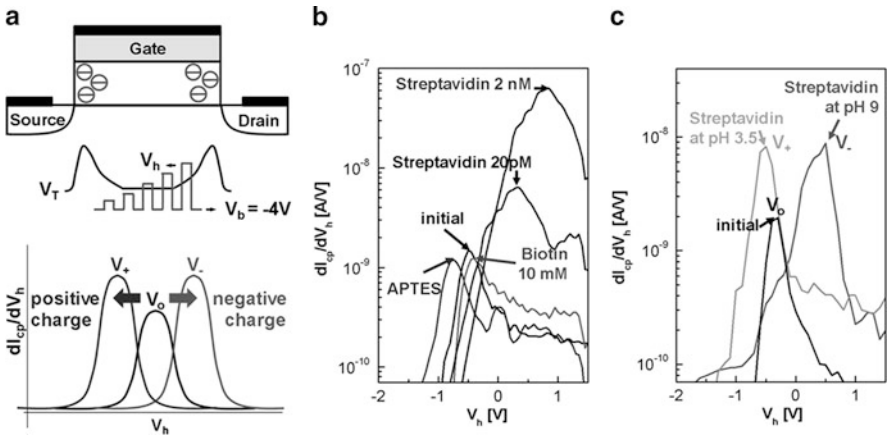

Fig. 5.21 (**a**) A schematic diagram showing the operating principle of the negatively charged biomolecules and the expected dI_{cp}/dV_h versus V_h [53]. (**b**) The dI_{cp}/dV_h versus V_h characteristics. The shift direction in the $dI_{cp}/dV_h - V_h$ plot indicates the charge polarity of the biomolecules [53]. (**c**) The measured dI_{cp}/dV_h data with two different pH solutions. When streptavidin is at pH 3.5, the expected charge polarity of streptavidin is positive. Therefore, the peak of $dI_{cp}/dV_h(V_+)$ is shifted to the left side from initial (V_0) value due to the locally increased V_T near the nanogap region (Copyright 2010 American Institute of Physics)

5.5.1.2 1/f Noise Measurement

The $1/f$ (flicker) noise in FET systems has been studied for more than four decades. It is known that the $1/f$ noise comes from the random trapping and detrapping processes of charges in the interface traps located at the Si/SiO_2 interface (channel/gate dielectric). The charge fluctuation results in fluctuation of the surface potential, which in turn modulates the channel carrier density and conductance. This type of noise is one of the limiting factors for biosensing. To distinguish the signal from noise clearly, the noise spectra in the frequency domain may allow contributions from different noise sources to be analyzed directly.

As shown in Fig. 5.22a, the concentration-dependent conductance change indicates that it is difficult to distinguish the signal from noise when the PSA concentration is at or below 0.15 pM. In contrast, when the device is in pure buffer, a clear $1/f$ spectrum (noise) can be observed in the frequency domain (Fig. 5.22b). When solutions of 0.15 pM PSA were delivered, the power spectra showed a curved-shape signal that was clearly different from that measured in buffer.

Therefore, the main benefit of $1/f$ noise technique is that sub-picomolar detection has been routinely achieved based on the fact that the characteristic frequencies associated with protein binding are well separated from other noise sources. An increase in the detection sensitivity of more than tenfold has been achieved with the frequency domain compared to time domain measurements from the same device.

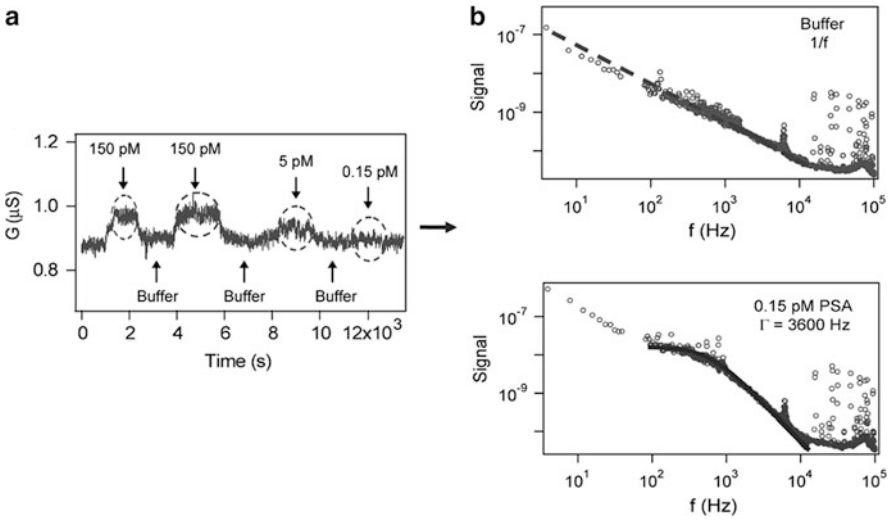

Fig. 5.22 (**a**) Time domain conductance measurement of a p-type Si nanowire FET sensor modified with PSA monoclonal antibodies. Different concentrations of PSA solutions and pure buffer were sequentially delivered to the sensor. *Dashed circles* indicate the time windows of PSA binding on the nanowire surface [54]. (**b**) The power spectrum of the same Si nanowire FET sensor in a buffer and in solutions with 0.15-pM PSA concentrations shows $1/f$ frequency dependence [54] (Copyright 2010 American Chemical Society)

The techniques described above, charge-pumping and $1/f$ noise measurement, were recently developed. Therefore, only a few preliminary studies of the techniques have been reported thus far. Both techniques demonstrated higher sensitivity compared to previous FET-based biosensors; however, the stability, reliability, and reproducibility of the biosensor operation have yet to be confirmed. In particular, the measurement procedure of both techniques is complicated, which could be problematic for their use in POCT systems. For the charge-pumping technique, a continuous pulse stream must be applied to the gate electrode, which requires an additional peripheral circuit to generate pulse. To measure the $1/f$ noise, additional equipment (generally an amplifier and a spectrum analyzer) is required for high-quality measurements, and these parts are not compatible with the miniaturization desired in POCT systems.

5.5.2 Substrate Current Method

Another parameter significantly affected by the status of the nanogap site in a DMFET is the substrate current (I_{sub}). The substrate current is generated when a high drain bias is applied while the channel is inverted. The high drain bias makes a high lateral electric field near the drain junction edge. Electrons accelerated by the

lateral electric field from the drain voltage trigger impact ionization, thus generating electron–hole pairs. The resulting electron–hole pairs are driven by the electric force produced by the applied bias on the substrate, and therefore, they create the substrate current, which is comprised of holes in an n-channel FET. Equations 5.6 and 5.7 express the substrate current and saturated drain voltage (V_{Dsat}) which predominantly affect the substrate current:

$$I_{sub} \propto (V_D - V_{Dsat}) I_D \exp\left(-\frac{B}{V_D - V_{Dsat}}\right) \tag{5.6}$$

$$V_{Dsat} = V_G - V_T \tag{5.7}$$

Here, B is the impact ionization coefficient [56]. The substrate current increases monotonically as V_G increases at a low or intermediated level of V_G because the first linear term on the right side in Eq. 5.6 is dominant over the substrate current. However, when V_G is very high, the substrate current is reduced by the second exponent term in Eq. 5.6. Thus, I_{sub} appears bell-shaped, with a crucial voltage ($V_G @ I_{sub,max}$) that shows the maximum I_{sub} value upon the first increment of I_{sub} led by an increase in the V_G value, with the next decrement of I_{sub} driven by the exponent decrease in Eq. 5.6. The $V_G @ I_{sub,max}$ value is significantly affected by the maximum electric field in which impact ionization occurs. Thus, the changed electric field near the gate edges, that is, near the drain junctions due to air and biomolecules in the nanogap, results in different $V_G @ I_{sub,max}$ values. The results as they pertain to the substrate current have yet to be reported, but I_{sub} could be one of the sensing parameters used in a DMFET.

5.6 Environmental Effect

Most previously reported biosensors were characterized under aqueous conditions [29, 47]. However, a few biomolecular detection experiments were also performed in ambient air environments [18, 30] (depending on the exposed condition, these are referred to as a "watery environment" or a "dry environment," respectively). Although measurements in a watery environment are common in biosensor characterizations because aqueous conditions maintain the functionality of biomolecules, measurements in a dry environment facilitate various device structures without consideration of the isolation between the aqueous solution and the device. Hence, characterizations of a biosensor in a bionic solution and in air ambient have been performed [57]. With the same device structure as an underlap FET, the researchers validated the biosensor functionality in a dry environment by comparing the result in watery environment.

To maintain biosensor operation in a bionic solution, an additional passivation layer that prevents leakage current through the bionic solution was implemented in the underlap FET, as shown in Fig. 5.23. The device was submerged in a bionic

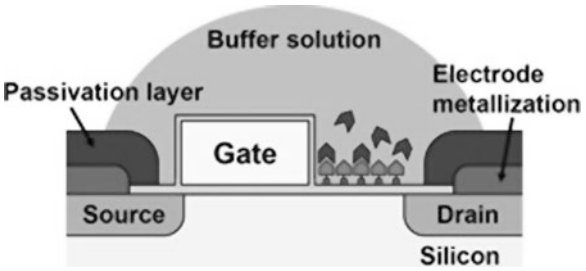

Fig. 5.23 The structure of an underlap FET with an additional layer for characterization in a wet environment

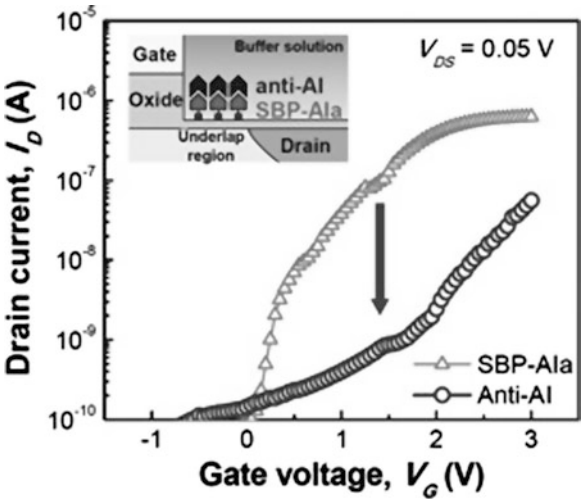

Fig. 5.24 Experimental results of an underlap FET in a wet environment. The drain current was decreased after anti-AI binding due to its negative charges at a pH of 7.4

solution or kept in ambient air for characterization in watery or dry environment, respectively.

As mentioned in Sect. 5.4.1, the channel potential of the underlap region is highly sensitive to the charge on it. An external charge on an open area will affect the drain current. Thus, a change in the drain current can be observed after target molecule binding in both wet and dry environments. The drain current reduction in the dry environment was shown in Sect. 5.4.1, and the result under the watery environment is demonstrated in Fig. 5.24. The drain current reduction in Fig. 5.24 can also explained by the electrical effect of the negatively charged biomolecules (anti-AI) in the underlap region.

To ensure the specific binding of anti-AI and AIa on the underlap FET, false-positive tests were performed in both watery and dry environments. First, a non-AIa-functionalized device was immersed in an anti-AI solution for 1 h; after which it was rinsed several times. As shown in Fig. 5.25, there was no change in the drain current for the nonfunctionalized device, even after anti-AI was added. In another control experiment, an AIa-functionalized device was exposed to an anti-rabbit-IgG antibody solution which showed nonspecific binding with AIa for 1 h; after which

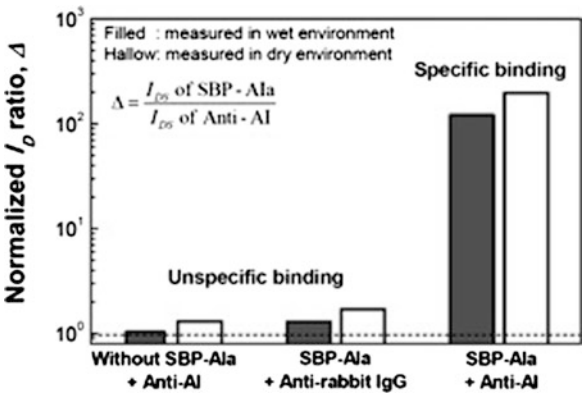

Fig. 5.25 Results of the control experiment for the specific binding test

it was rinsed several times. This experiment also resulted in a negligible change in the drain current as expected. The results clearly confirmed that the considerable decrease in the drain current for both environments was due to the specific binding of anti-AI and AIa. Thus, it was verified that the biosensor characteristics measured in dry environments are valid to the same extent as they are in watery environments.

Acknowledgements This work was supported by the National Research and Development Program under grant NRDP, 2012-0001131 for the development of biomedical function monitoring biosensors and by the Center for Integrated Smart Sensor through the National Research Foundation of Korea funded by the Ministry of Education, Science, and Technology under Grant CISS-2011-0031845.

References

1. J. Wang, Electrochemical biosensors: towards point-of-care cancer diagnostics. Biosens. Bioelectron. **21**(10), 1887–1892 (2006)
2. L.J. Kricka, Nucleic acid detection technologies – labels, strategies, and formats. Clin. Chem. **45**(4), 453–458 (1999)
3. J. Fritz, E.B. Cooper, S. Gaudet, P.K. Sorger, and S.R. Manalis, Electronic detection of DNA by its intrinsic molecular charge. Proc. Natl. Acad. Sci. U.S.A. **99**, 14142–14146 (2002)
4. J.R. Macdonald (ed.), *Impedance Spectroscopy* (Wiley, New-York, 1987)
5. I. Rubinstein (ed.), *Physical Electrochemistry: Principle, Method and Applications* (Marcel Dekker, New-York, 1995)
6. J. Rickert, W. Göpel, W. Beck, G. Jung, and P. Heiduschka, A 'mixed' self-assembled monolayer for an impedimetric immunosensor. Biosens. Bioelectron. **11**(8), 757–768 (1996)
7. S. Hleli, C. Martelet, A. Abdelghani, N. Burais, and N. Jaffrezic-Reuault, Atrazine analysis using an impedimetric immunosensor based on mixed biotinylated self-assembled monolayer. Sens. Actuators B **113**(2), 711–717 (2006)
8. C. Ruan, L. Yang, and Y. Li, Immunobiosensor chips for detection of *Escherichia coli* O157:H7 using electrochemical impedance spectroscopy. Anal. Chem. **74**(18), 4814–4820 (2002)
9. F. Patolsky, A. Lichtenstein, and I. Willner, Detection of single-base DNA mutations by enzyme-amplified electronic transduction. Nat. Biotechnol. **19**(3), 253–257 (2001)

10. W. Cai, J.R. Peck, D.W. van der Weide, and R.J. Hamers, "Direct electrical detection of hybridization at DNA-modified silicon surfaces. Biosens. Bioelectron. **19**(9), 1013–1019 (2004)
11. F. Lucarelli, G. Marrazza, A.P.F. Turner, and M. Mascini, Carbon and gold electrodes as electrochemical transducers for DNA hybridisation sensors. Biosens. Bioelectron. **19**(6), 515–530 (2004)
12. L. Alfonta, A.K. Singh, and I. Willner, Liposomes labeled with biotin and horseradish peroxidase: a probe for the enhanced amplification of antigen-antibody or oligonucleotide – DNA sensing processes by the precipitation of an insoluble product on electrodes. Anal. Chem. **73**(1), 91–102 (2001)
13. F. Patolsky, A. Lichtenstein, and I. Willner, Electrochemical transduction of liposome-amplified DNA sensing. Angew. Chem. Int. Ed. **39**(5), 940–943 (2000)
14. F. Patolsky, A. Lichtenstein, and I. Willner, Electronic transduction of DNA sensing processes on surfaces: amplification of DNA detection and analysis of single-base mismatches by tagged liposomes. J. Am. Chem. Soc. **123**(22), 5194–5205 (2001)
15. O. Ouerghi, A. Senillou, N. Jaffrezic-Renault, C. Martelet, H. Ben Ouada, and S. Cosnier, Gold electrode functionalized by electropolymerization of a cyano N-substituted pyrrole: application to an impedimetric immunosensor. J. Electroanal. Chem. **501**(1-2), 62–69 (2001)
16. Y. Xu, H. Cai, P.-G. He, and Y.-Z. Fang, Probing DNA hybridization by impedance measurement based on CdS-oligonucleotide nanoconjugates. Electroanalysis **16**(1-2), 150–155 (2004)
17. J. Wang, J.A. Profitt, M.J. Pugia, and I.I. Suni, Au nanoparticle conjugation for impedance and capacitance signal amplification in biosensors. Anal. Chem. **78**(6), 1769–1773 (2006)
18. A. Star, J.-C.P. Gabriel, K. Bradley, and G. Grüner, Electronic detection of specific protein binding using nanotube FET devices. Nano Lett. **3**(4), 459–463 (2003)
19. A. Kim, C.S. Ah, H.Y. Yu, J.-H. Yang, I.-B. Baek, C.-G. Ahn, C. W. Park, M.S. Jun, and S. Lee, Ultrasensitive, label-free, and real-time immunodetection using silicon field-effect transistors. Appl. Phys. Lett. **91**(10), 103901 (2007)
20. P. Bergveld, Development, operation and application of the ion-sensitive field-effect transistor as a tool for electrophysiology. IEEE Trans. Biomed. Eng. **BME-19**(5), 342–351 (1972)
21. H.H. Van den Vlekkert et al., A pH-ISFET and an integrated pH-pressure sensor with back-side contacts. Sens. Actuator **14**(2), 165–176 (1988)
22. J.C. Chou, C.N. Hsiao, The hysteresis and drift effect of hydrogenated amorphous silicon for ISFET. Sens. Actuators B **66**(1-3), 181–183 (2000)
23. O. Leistiko, The selective and temperature characteristics of ion sensitive field effect transistors. Phys. Scr. **18**(6), 445–450 (1978)
24. Y. Cui, Q. Wei, H. Park and C.M. Lieber, Nanowire nanosensors for highly sensitive and selective detection of biological and chemical species. Science **293**(5533), 1289–1292 (2001)
25. W.U. Wang, C. Chen, K.-H. Lin, Y. Fang, Y. and C.M. Lieber, Label-free detection of small-molecule-protein interactions by using nanowire nanosensors. Proc. Natl. Acad. Sci. U.S.A. **102**(9), 3208–3212 (2005)
26. G. Zheng, F. Patolsky, Y. Cui, W.U. Wang, and C.M. Lieber, Multiplexed electrical detection of cancer markers with nanowire sensor arrays. Nat. Biotechnol. **23**(10), 1294–1301 (2005)
27. J.-I. Hahm, and C.M. Lieber, Direct ultrasensitive electrical detection of DNA and DNA sequence variations using nanowire nanosensors. Nano Lett. **4**(1), 51–54 (2004)
28. F. Parolsky, G. Zheng, O. Hayden, M. Lakadamyali, X. Zhuang and C.M. Lieber, Electrical detection of single viruses. Proc. Natl. Acad. Sci. U.S.A. **101**(39), 14017–14022 (2004)
29. E. Stern, J.F. Klemic, D.A. Routenberg, P.N. Wyrembak, D.B.T.-Evans, A.D. Hamilton, D.A. LaVan, T.M. Fahmy and M.A. Reed, Label-free immunodetection with CMOS-compatible semiconducting nanowires. Nature **445**(2), 519–522 (2007)
30. H. Im, X.-J. Haung, B. Gu and Y.-K. Choi, A dielectric-modulated field-effect transistor for biosensing. Nat. Nanotech. **2**(7), 430–434 (2007)
31. B. Gu, T.J. Park, J.-H. Ahn, X.-J. Huang, S.Y. Lee, and Y.-K. Choi, Nanogap field-effect transistor biosensors for electrical detection of avian influenza. Small **5**(21), 2407–2412 (2009)

32. M. Im, J.-H. Ahn, J.-W. Han, T.J. Park, S.Y. Lee, Y.-K. Choi, Development of a point-of-care testing platform with a nanogap-embedded separated double-gate field effect transistor array and its readout system for detection of avian influenza. IEEE Sens. J. **11**(2), 351–360 (2011)
33. R.B. Schoch, J. Han, and P. Renaud, Transport phenomena in nanofluidics. Rev. Mod. Phys. **80**(3), 839–883 (2008)
34. A. Bezryadin, and C. Dekker, Nanofabrication of electrodes with sub-5 nm spacing for transport experiments on single molecules and metal clusters. J. Vac. Sci. Technol. B **15**(4), 793–799 (1997)
35. D. Porath, A. Bezryadin, S. de Vries, and C. Dekker, Direct measurement of electrical transport through DNA molecules. Nature **403**(6770), 635–638 (2000)
36. S.M. Sze, *Physics of Semiconductor Devices*, 2nd edn. (Wiley, New York, 1981)
37. G.D. Wilk, R.M. Wallace, and J.M. Anthony, High-κ dielectrics: current status and materials properties considerations. J. Appl. Phys. **89**(10), 5243–5275 (2001)
38. C.-H. Kim, C. Jung, K.-B. Lee, H.G. Park, and Y.-K. Choi, Label-free DNA detection with a nanogap embedded complementary metal oxide semiconductor. Nanotechnology **22**(13), 1032–1039 (2011)
39. K.-W. Lee, S.-J. Choi, J.-H. Ahn, D.-I. Moon, T.J. Park, S.Y. Lee, Y.-K. Choi, An underlap field-effect transistor for electrical detection of influenza. Appl. Phys. Lett. **96**(3), 033703 (2010)
40. B. Bhushan, (ed.), *Springer Handbook of Nanotechnology* (Springer, Heidelberg, 2004)
41. G.-J. Zhang, J.H. Chua, R.-E. Chee, A. Agarwal, and S.M. Wong, Label-free direct detection of MiRNAs with silicon nanowire biosensors. Biosens. Bioelectron. **24**(8), 2504–2508 (2009)
42. J.-H. Ahn, S.-J. Choi, J.-W. Han, T.J. Park, S.Y. Lee, and Y.-K. Choi, Double-gate nanowire field effect transistor for a biosensor. Nano Lett. **10**(8), 2934–2938 (2010)
43. M. Masahara, Y. Liu, K. Sakamoto, K. Endo, T. Mausukawa, K. Ishii, T. Sekigawa, H. Yamauchi, H. Tanoue, S. Kanemaru, H. Koike, and E. Suzuki, Demonstration, analysis, and device design considerations for independent DG MOSFETs. IEEE Trans. Electron. Devices **52**(9), 2046–2053 (2005)
44. O. Knopfmacher, A. Tarasov, W. Fu, M. Wipf, B. Niesen, M. Calame, and C. Schönenberger, Nernst limit in dual-gated Si-nanowire FET sensors. Nano Lett. **10**(6), 2268–2274 (2010)
45. M.T. Martinez, Y.–C. Tseng, N. Ormategui, I. Loinaz, R. Eritja, and J. Bokor, Label-free DNA biosensors based on functionalized carbon nanotube field effect transistors. Nano Lett. **9**, 530–536 (2009)
46. I. Heller, J. Mannik, S.G. Lemay, and C. Dekker, Optimizing the signal-to-noise ratio for biosensing with carbon nanotube transistors. Nano Lett. **9**, 377–382 (2009)
47. N. Elfstrom, R. Juhasz, I. Sychugov, T. Engfeldt, A.E. Karlstrom, and J. Linnros, Surface charge sensitivity of silicon nanowires: size dependence. Nano Lett. **7**, 2608–2612 (2007)
48. J.S. Brugler, and P.G.A. Jespers, Charge pumping in MOS devices. IEEE Trans. Electron. Devices **ED-16**, 297–302 (1969)
49. P. Dutta, and P.M. Horn, Low-frequency fluctuations in solids: 1/f noise. Rev. Mod. Phys. **53**, 497–516 (1981)
50. S. Kim, J.–H. Ahn, T.J. Park, S.Y. Lee, and Y.–K. Choi, A biomolecular detection method based on charge pumping in a nanogap embedded field-effect-transistor biosensor. Appl. Phys. Lett. **94**, 243903 (2009)
51. S. Kim, J.–H. Ahn, T.J. Park, S.Y. Lee, and Y.–K. Choi, Charge pumping technique to analyze the effect of intrinsically retained charges and extrinsically trapped charges in biomolecules by use of a nanogap embedded biotransistor. Appl. Phys. Lett. **96**, 053702 (2010)
52. S. Kim, J.–H. Ahn, T.J. Park, S.Y. Lee, and Y.–K. Choi, Comprehensive study of a detection mechanism and optimization strategies to improve sensitivity in a nanogap-embedded biotransistor. J. Appl. Phys. **107**, 114705 (2010)
53. S. Kim, J.–Y. Kim, J.–H. Ahn, T.J. Park, S.Y. Lee, and Y.–K. Choi, A charge pumping technique to identify biomolecular charge polarity using a nanogap embedded biotransistor. Appl. Phys. Lett. **97**, 073702 (2010)

54. G. Zheng, X.P.A. Gao, and C.M. Lieber, Frequency domain detection of biomolecules using silicon nanowire biosensors. Nano Lett. **10**, 3179–3183 (2010)
55. G. Groeseneken, H.E. Maes, N. Beltran, and R.F. Keersmaecker, A reliable approach to charge-pumping measurements in MOS transistors. IEEE Trans. Electron. Devices **ED-31**, 42–53 (1984)
56. R.S. Muller, T.I. Kamins, M. Chan, *Device Electronics for Integrated Circuits*. 3rd edn. (Willey, New York, 2002), pp. 490–495
57. J.-Y. Kim, J.-H. Ahn, S.-J. Choi, M. Im, S. Kim, J. P. Duarte, C.-H. Kim, T. J. Park, S. Y. Lee, and Y.-K. Choi, An underlap channel-embedded field-effect fransistor for biosensor application in watery and dry environment, IEEE Trans. Nanotechnol. **11**(2), 390–394 (2012)